Tunable magnetic scattering and ferroelectric switching at the $LaAlO_3/EuTiO_3/Sr_{0.99}Ca_{0.01}TiO_3$ interface

G. Tuvia,[1] S. W. Sobelman,[2] S. Sandik,[1] B. Kalisky,[2,*] and Y. Dagan[1,†]

[1]*School of Physics and Astronomy, Tel-Aviv University, Tel Aviv 6997801, Israel*

[2]*Department of Physics and Institute of Nanotechnology and Advanced Materials, Bar-Ilan University, Ramat-Gan 5290002, Israel*

(Received 24 March 2022; accepted 8 July 2022; published 26 July 2022)

Ferroelectric and ferromagnetic orders rarely coexist, and magnetoelectric coupling is even more scarce. A possible avenue for combining these orders is by interface design, where orders formed at the constituent materials can overlap and interact. Using a combination of magnetotransport and scanning superconducting quantum interference device measurements, we explore the interactions between ferroelectricity, magnetism, and the two-dimensional electron system (2DES) formed at the novel $LaAlO_3/EuTiO_3/Sr_{0.99}Ca_{0.01}TiO_3(001)$ heterostructure. We find that the electrons at the interface experience magnetic scattering appearing along with a diverging Curie-Weiss-type behavior in the $EuTiO_3$ layer. The 2DES is also affected by the switchable ferroelectric polarization at the $Sr_{0.99}Ca_{0.01}TiO_3$ bulk. While the 2DES interacts with both magnetism and ferroelectricity, we show that the presence of the conducting electrons has no effect on magnetization in the $EuTiO_3$ layer. Our results provide a first step towards realizing a new multiferroic system where magnetism and ferroelectricity can interact via an intermediate conducting layer.

DOI: 10.1103/PhysRevMaterials.6.074408

I. INTRODUCTION

Materials exhibiting ferroelectricity and ferromagnetism have been long-sought because of their potential use in multifaceted memory devices. However, long-range orders such as ferroelectricity, ferromagnetism, and superconductivity rarely coexist. For example, ferroelectricity often requires empty *d* orbitals, while conventional ferromagnets require partially filled *d* orbitals [1]. Superconductivity and ferroelectricity also seem mutually exclusive due to the inversion symmetry breaking needed for the latter [2]. A possible avenue for combining seemingly incompatible orders is by interface design, where orders formed at the constituent materials can overlap. This approach has been successful in combining ferroelectricity and ferromagnetism by designing composite heterostructures [3]. Furthermore, a two-dimensional (2D) superconductor was recently realized at the interface of a ferroelectric Ca-substituted $SrTiO_3$ crystal [4]. The incorporation of ferroelectricity to conducting interfaces raises the possibility of controlling other properties, such as magnetism by ferroelectric switching.

In its bulk form, $EuTiO_3$(ETO) is a G-type antiferromagnet with a Néel temperature of 5.5 K [5–7]. However, when strained [8] or doped [9–15] it becomes ferromagnetic with Curie temperatures ranging from 4–12 K. The emergence of a ferromagnetic phase by straining is explained by a change of magnetic exchange parameters [16]. Straining also drives ETO into a ferroelectric phase [8], making it a candidate system for multiferroic research. Doping-induced magnetism on the other hand, is believed to result from Ruderman-Kittel-Kasuya-Yosida (RKKY) interactions [13–15,17].

ETO is isomorphic to $SrTiO_3$(STO). It has been shown that one-or two-unit cells of ETO can be grown between STO and $LaAlO_3$(LAO) without destroying the conducting interface [18], which is well known to form at the LAO/STO interface [19] with various explanations for its origin [19–21]. The resulting LAO/ETO/STO heterostructure displays gate tunable superconductivity and non-linear Hall resistivity below 10 K suggested to originate from a tunable ferromagnetic phase [18].

Here, we report magnetotransport of the $LaAlO_3/EuTiO_3/Sr_{0.99}Ca_{0.01}TiO_3(001)$ (LAO/ETO/CSTO) heterostructure combined with local mapping of electrical currents and magnetism using scanning superconducting quantum interference device (SQUID) microscopy. We find a diverging Curie-Weiss-type susceptibility at low temperatures appearing along with with a $\ln(\frac{1}{T})$ term in the sheet resistance. We interpret the magnetoelectric-transport properties in the framework of a 2D polar metal affected by scattering off magnetic fluctuations. Ferroelectricity also interacts with the 2D electron system (2DES) as demonstrated by the hysteresis observed in sheet resistance and magneto-transport when switching ferroelectric polarization in the bulk. Our results demonstrate that a 2D electron system can be designed to interact with ferroelectricity and magnetism. While the 2DES is affected by both the bulk ferroelectricity and the magnetic ETO layer, we find that the presence of the conduction electrons has no effect on the ETO magnetism.

II. RESULTS

A. Heterostructure design

Our goal in this work is to realize a conducting interface exhibiting both ferroelectric and magnetic properties. To design such a system we chose three components:

*Corresponding author: beena@biu.ac.il

†Corresponding author: yodagan@tauex.tau.ac.il

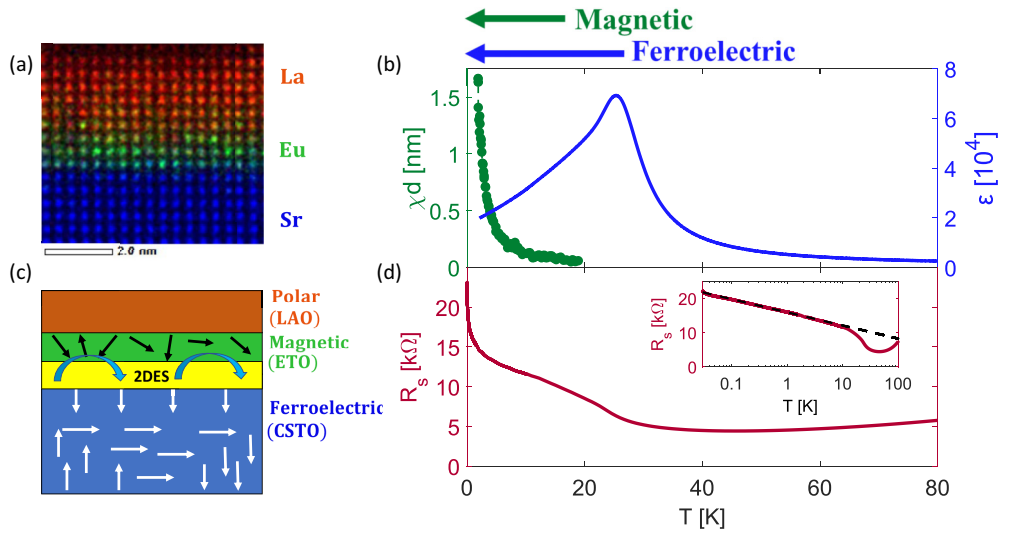

FIG. 1. Magnetism and ferroelectricity interacting with the 2DES: (a) STEM measurement along with EELS elemental identification confirming the high quality growth of the interface. (b) Green (left scale): Magnetic susceptibility versus temperature, showing a Curie-Weiss behavior originating from the ETO layer. Blue (right scale): Dielectric constant of the CSTO substrate. A ferroelectric transition is observed at ∼30 K. (c) Sketch of our understanding of the system: The 2D polar metal is controllable by switching the bulk ferroelectricity and experiences scattering from spin fluctuations in the ETO layer. (d) Interface sheet resistance versus temperature. Inset: Sheet resistance versus temperature in logarithmic scale, highlighting the $\ln(\frac{1}{T})$ behavior at low temperatures.

(1) Ferroelectric CSTO, which will serve as the substrate for the heterostructure.

(2) A thin two-unit cell layer of magnetic ETO.

(3) Eight-unit cells of LAO, which induce conductivity at the interface.

The resulting heterostructure can be seen in figure 1(a), where we show scanning-transmission-electron-microscopy (STEM) imaging along with electron-energy-loss-spectroscopy (EELS) measurements, verifying the expected structure and composition of our heterostructure (further details are shown in Fig. S1 in the Supplemental Material [22]).

The interface is metallic at high temperatures [Fig. 1(d)]. Upon further cooling of the heterostructure, two distinct features can be observed: an upturn to the resistance below the ferroelectric transition, and a $\ln(\frac{1}{T})$ term becoming dominant at low temperatures [highlighted in inset of Fig. 1(d)]. As we elaborate below, we relate both of these terms to interactions of the 2DES with the ferroelectric bulk and the magnetic ETO layer.

B. Ferroelectricity

We begin by characterizing ferroelectricity in the bulk CSTO crystal. The dielectric constant is extracted by capacitance measurements and is presented in Fig. 1(b) (blue). A ferroelectric transition is observed at ∼30 K, as expected for one percent Ca substitution [23].

The ferroelectric transition has a dramatic effect on the interface resistance. As can be seen in Fig. 1(d), the interface resistance increases as temperature is lowered into the ferroelectric phase. We have previously interpreted an upturn in resistance below the ferroelectric transition as a result of an effective gate bias exerted by the ferroelectric bulk, acting to deplete carriers from the interface as the temperature is lowered [4]. Furthermore, as temperature is lowered deeper into the ferroelectric phase, resistance versus back-gate voltage hysteresis loops are observed (Fig. 2), demonstrating

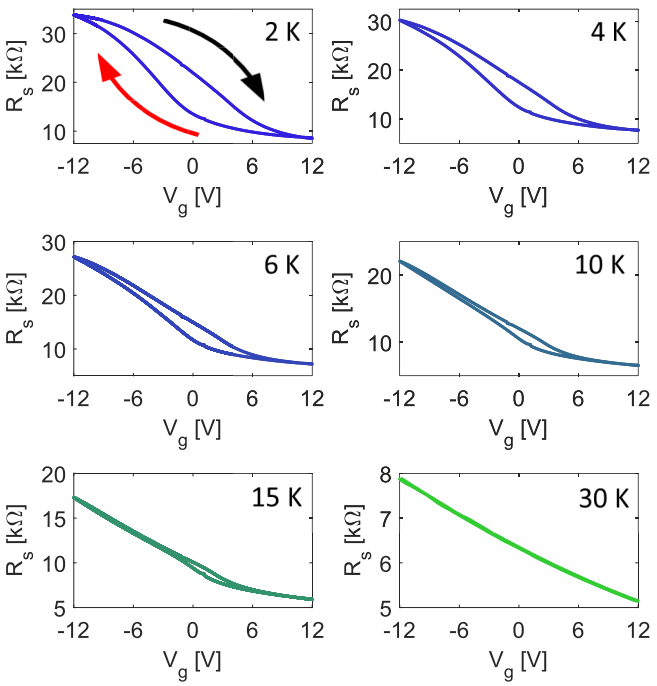

FIG. 2. Temperature evolution of resistance versus gate hysteresis. Sheet resistance response to applied back-gate voltage shows hysteretic behavior below the ferroelectric transition. This hysteresis becomes larger as temperature is lowered deeper into the ferroelectric phase, demonstrating control of interface resistance by ferroelectric switching.

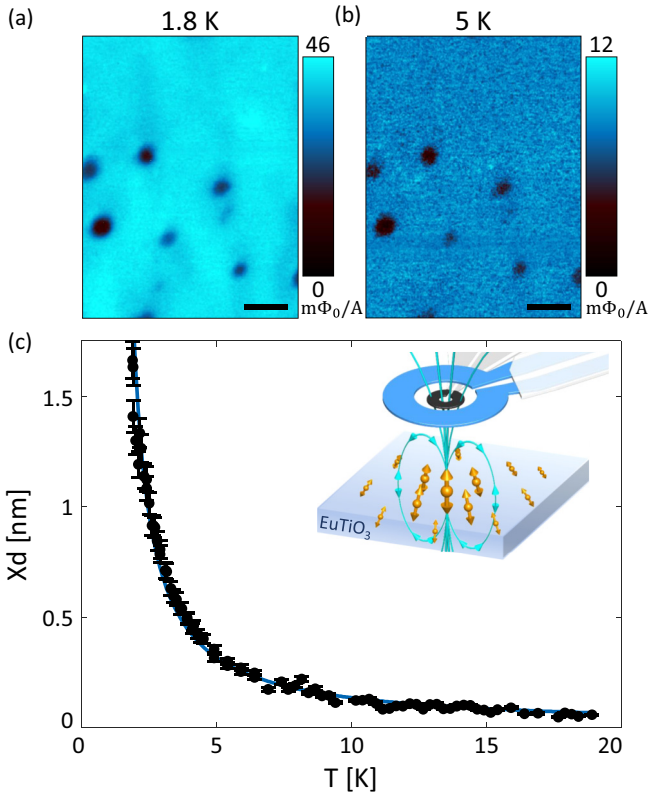

FIG. 3. The paramagnetic-type signal decays with the temperature. (a), (b) Maps of the paramagnetic-type response at 1.8 K (a) and 5 K (b). Scale bars 20 m; (c) Paramagnetic susceptibility as a function of the temperature. Inset: Illustration of the SQUID susceptometry measurement.

ferroelectric control of the 2DES. The area of these loops increases as temperature is lowered, as previously reported for 2D polar metals formed at CSTO-based interfaces [4,24].

C. Magnetism

In Figs. 3(a) and 3(b) we present spatial susceptibility measurements of our interface at 1.8 and 5 K, respectively. The signal is mostly isotropic and only changes at imperfections on the interface [black regions in Figs. 3(a) and 3(b)], where the magnetic signal, as well as the conductivity, are substantially weaker (see Fig. S2 in the Supplemental Material [22] for more details).

To quantify the evolution of the magnetic signal with temperature, we perform a Curie-Weiss fit to the susceptibility measurements [solid line in Fig. 3(c)]:

$$\frac{1}{\chi d} = \frac{3K_B}{\mu_0(g\mu_B)^2 J(J+1)}\frac{1}{n_s}(T - T_C),$$

where χ is the unitless susceptibility, d is the thickness of the magnetic layer, J is the nuclear spin number, n_s is the spin density and T_C is the Curie temperature.

We can now extract the spin density n_s from the fit to find the origin of the magnetic response. If we assume $J = \frac{7}{2}$ (i.e., that the magnetic signal originates from the Eu atoms) we receive a spin density of $n_s = 8.2 \times 10^{14}\ \frac{1}{\text{cm}^2}$, which is the expected order of the number of Eu atoms. However, if we assume $J = \frac{1}{2}$ (i.e., that the magnetic signal originates from the 2DES), we receive a spin density of $n_s = 1.7 \times 10^{16}\ \frac{1}{\text{cm}^2}$, which can be ruled out since it is two orders of magnitude larger than the overestimated carrier density of half an electron per unit cell [19].

We note that the spin densities calculated here are lower limits as the susceptibility was measured with respect to the imperfections on the sample, which have a much weaker yet nonzero signal. By subtracting the background signal away from the sample we can set a more realistic estimation for the signal of $1.4 \times 10^{15}\ \frac{1}{\text{cm}^2}$ for $J = \frac{7}{2}$. However, this estimation is hindered by noise (experimental limitations, see Figure S3 in Supplemental Material [22] for more information). We therefore conclude that for $J = \frac{7}{2}$, the spin density is larger than 8.2×10^{14}, likely around $1.4 \times 10^{15}\ \frac{1}{\text{cm}^2}$. This value is in excellent agreement with the expected density of Eu atoms within two-unit cells of ETO ($1.3 \times 10^{15}\ \frac{1}{\text{cm}^2}$), further confirming that the magnetic signal originates from the ETO layer.

The Curie-Weiss behavior persists down to 1.7 K (our SQUID experimental base temperature), with no clear signs of a magnetic phase transition. The Curie temperature extracted from the fit shown in Fig. 3(c) is 0.9 K. However, with an error of 0.7 K, this number does not provide reliable information regarding a phase transition.

Interestingly, the $\ln(\frac{1}{T})$ term observed in the interface resistance becomes dominant at the same temperature range where the susceptibility diverges. We interpret this behavior as a signature of magnetic fluctuations in the ETO layer scattering conduction electrons in the 2DES. This view is consistent with the magnetoresistance (MR) measurements showed below.

In Fig. 4(a), we present resistance versus magnetic field measurements with field perpendicular to the interface at different temperatures. The sign of the MR depends on both field magnitude and temperature. We interpret this behavior as a result two competing effects: A negative spin MR, resulting from interactions with the magnetic ETO layer, and a positive, orbital quadratic term. At low temperatures, the spin component is stronger while at sufficiently high magnetic fields, the quadratic component dominates.

To quantify the spin and orbital contributions, we rotate the sample at a constant magnetic field of 14 T. The resulting MR(θ) measurements are presented in Fig. 4(b), where θ is the angle between the field and the interface. For $70^\circ \leqslant \theta \leqslant 110^\circ$, we assume that the magnetic anisotropy is negligible, hence we fit the data in this regime to $\alpha + \beta \times \text{Sin}^2(\theta)$, where α and β are constants representing the magnitude of the spin and orbital effects, respectively. The resulting orbital component is presented in Fig. S8 in the Supplemental Material [22]. We then subtract this positive component from the original signal to obtain the spin contribution [Fig. 4(c)]. We find that the spin component is negative and becomes stronger as the temperature is lowered, as expected for magnetic fluctuations increasing at low temperatures. Furthermore, we observe an anisotropy of the spin component as θ approaches zero (in-plane magnetic field), reflecting the 2D nature of the ETO layer.

The magnitude of both spin and orbital components can be tuned by gate voltage. This is demonstrated in Fig. 4(d) where

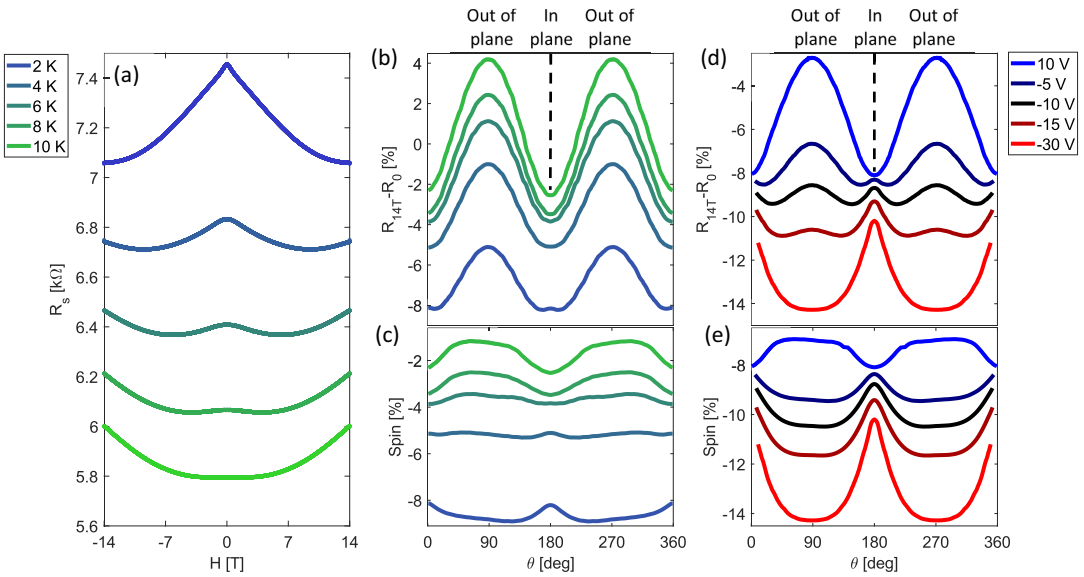

FIG. 4. Low temperature magnetoresistance (MR) measurements. (a) Symmetrized resistance versus out-of-plane magnetic field for different temperatures. (b) MR magnitude at 14 T for different temperatures and angles between the interface and the field (θ). (c) MR magnitude after subtraction of extrapolated orbital effect. This remaining effect illustrates the MR spin component. (d) MR magnitude at 2 K for different back-gate voltages and angles θ. (e) Gate-dependant spin contribution achieved similarly to (c). This term becomes more dominant at negative gates (electron depletion).

we performed field rotation measurements at 2 K at various gate voltages. Using similar analysis as in Figs. 4(b) and 4(c), we find that the spin component increases in magnitude as electrons are depleted (negative gate voltage) from the 2DES [Fig. 4(e)]. As we elaborate in the discussion section, we relate this result to a change in position of the 2DES relative to the interface as function of carrier concentration.

We note that the spin-MR does not saturate at magnetic fields as high as 14 T. To further demonstrate this, we show in Fig. S9 in the Supplemental Material [22] low temperatures measurements of resistance versus in-plane magnetic field, where the orbital effect is not expected. No saturation of the MR is observed.

To demonstrate control of these magnetic scattering effects by ferroelectric switching, we stabilize a resistance versus back-gate voltage hysteresis loop at 2 K, as can be seen in Fig. 5(a). We measured the MR at zero gate bias, for different sweep directions: coming from positive bias (red) and from negative bias (black). To estimate the spin-MR we performed an analysis similar to that presented in Fig. 4. Despite the zero gate bias, the MR is significantly altered due to the memory effect of the ferroelectric polarization.

While the results presented above point to magnetic fluctuations in the ETO layer scattering electrons in the 2DES, we find no evidence of the 2DES altering magnetism in the ETO layer, as one would expect from an RKKY-type magnetism. This can be seen in Fig. S7 in the Supplemental Material [22], where susceptibility maps are measured at different back-gate voltages. We find that the susceptibility is independent on carrier density within resolution.

To further examine the effect of conduction electrons on magnetism, we performed similar scanning SQUID measurements for nonferroelectric LAO/ETO/STO hetereostructes. Two samples were studied: A conducting sample with a two-unit-cell thick layer of ETO at the interface and another sample with five-unit cells of ETO, which results in an insulating interface. Susceptibility versus back-gate voltage measurement were performed for the conducting sample, showing no effect of carrier modulation on the magnetic response (Fig. S7 in the Supplemental Material [22]). We note that our transport study reproduce previous results on the LAO/ETO/STO interface [18] (Fig. S5 in the Supplemental Material [22]). The insulating sample studied here shows qualitatively similar results to the conducting samples (Fig. S6(b) in the Supplemental Material [22]). These results further imply that the 2DES formed at these interfaces does not play a role in inducing magnetism in the thin ETO layer.

We now move to the question of the magnetic ground state of the thin ETO layer. For either a ferromagnetic or antiferromagnetic phase transition, one would expect a saturation of the magnetic susceptibility below the transition temperature. However, no such saturation is observed, suggesting that the ETO does not undergo magnetic ordering down to 1.7 K. This observation is further supported by the zero-field spatial magnetic imaging produced at 1.7 K, which shows no evidence of ferromagnetic domains (Fig. S2(a) in the Supplemental Material [22]). An in-plane aligned magnetization is also ruled out, since fringing field lines from such domains would have been picked up at the presumed domain boundaries. These observations also hold for the nonferroelectric LAO/ETO/STO interfaces studied here (see Figs. S2(b), S2(c), and S6 in the Supplemental Material [22]).

No clear indication of a magnetic phase transition is visible in transport. This can be seen by the $\ln(\frac{1}{T})$ upturn to the interface resistance, showing no saturation down $\sim$20 mK. Typically, magnetic ordering is accompanied by a saturation of such a resistance upturn, as can be observed for example in systems such as doped ETO [11–14] and manganites

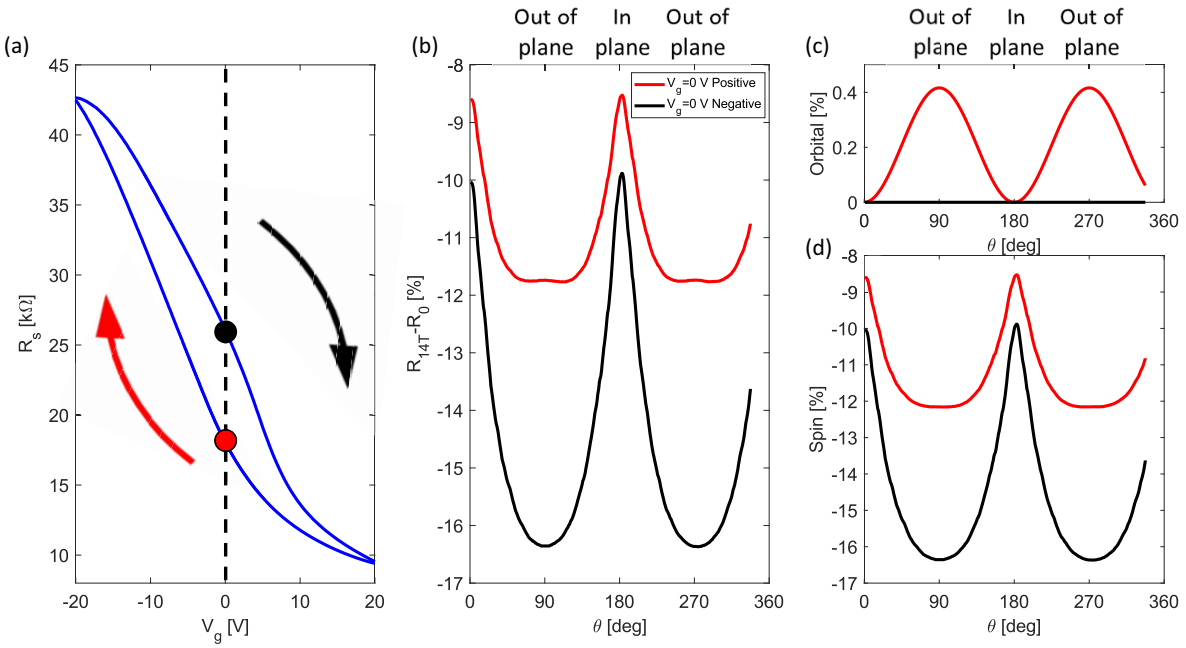

FIG. 5. Tuning magnetic scattering with ferroelectric memory. (a) Sheet resistance versus back-gate voltage hysteresis loop at 2 K. Red/black dots mark the zero-gate positive/negative points of the loop where measurements shown in (b)–(d) were taken. (b) MR magnitude at 14 T for different angles between the interface and the field (θ). These measurements were taken at zero-gate voltage for the positive/negative sides of the loop shown in (a). (c) Fitted orbital term for angles near the out-of-plane orientation ($80^\circ \leqslant \theta \leqslant 100^\circ$) (d) MR magnitude after subtraction of extrapolated orbital effect (c).

[25,26]. Furthermore, no magnetic hysteresis is visible at 0.5 K (Fig. S4 in the Supplemental Material [22]), as opposed to, for example, the case of Sm doped ETO, which shows a strong hysteresis below the Curie temperature [14].

III. DISCUSSION

In Fig. 1(c) we sketch our understanding of how ferroelectricity and magnetism interact with the 2DES in the LAO/ETO/CSTO heterostructure. The conduction electrons reside at the edge of the ferroelectric CSTO and are adjacent to the magnetic ETO layer. Ferroelectricity in the CSTO bulk can be switched by using the gate voltage to control the 2DES properties (Fig. 2). The sketched ferroelectric domain structure is presumed to be similar to that of the LAO/CSTO system (see Ref. [4] for more information). As the temperature is lowered, magnetic fluctuations in the ETO layer increase and scatter the conduction electrons in the 2D polar metal. This scattering results in a strong negative spin-MR signal (Fig. 4) and a Kondo-type temperature dependence of the resistivity [Fig. 1(d)] appearing together with a divering Curie-Weiss behavior of the ETO susceptibility [Fig. 3(c)]. We note that similar Kondo-type temperature dependence of the resistance and negative MR were previously observed in doped ETO [11–14] in manganites [25,26] and in electron-doped cuprates [27].

Furthermore, we show the spin MR term can be tuned by applying back-gate voltages, becoming stronger at negative gates [electron depletion, Fig. 4(e)]. We explain this enhancements by the 2DES becoming spatially closer to the ETO layer, making the 2DES more susceptible to magnetic scatterings. This picture of the electrons becoming more confined to the interface at the depleted regime is in line with the calculation of Delugas *et al.* [28].

Since ferroelectric switching controls the 2DES in a hysteretic fashion, we were able to tune magnetic scatterings by ferroelectric memory as shown in Fig. 5. The ability to control magnetic properties with ferroelectric memory aligns well with previous works on CSTO showing control of sheet resistance [4,24] and superconductivity [4] by ferroelectric switching of polarization in the bulk crystal.

While the 2DES experiences scattering off magnetic fluctuations originating in the ETO layer, our observations show that the magnetism in the ETO layer is unaffected by the presence of the 2DES. This conclusion is supported by the following observations: (1) The magnetic susceptibility is independent of gate voltage (Fig. S7 in the Supplemental Material [22]). (2) Non-conducting ETO based heterostructures show qualitatively similar magnetic measurements to the conducting samples (Figs. S2 and S6 in the Supplemental Material [22]). (3) All ETO-based samples studied here exhibit no ferromagnetism (Figs. S2 (a)–S2(c) in the Supplemental Material [22]).

Recently, LAO/STO interfaces were fabricated with $GdTiO_3$ interlayers instead of $EuTiO_3$ [29]. These interfaces present similar, gate-tunable non-linear Hall signatures to those observed in the LAO/ETO/STO interface. However, no ferromagnetic domains were found in scanning SQUID measurements.

IV. METHODS

A. Sample preparation and transport measurements

Two-unit cells of $EuTiO_3$ followed by eight-unit cells of $LaAlO_3$ were deposited by pulsed laser deposition on atomically flat TiO_2 terminated $Sr_{0.99}Ca_{0.01}TiO_3$ substrates. Both ETO and LAO were deposited *in situ* at a rate of 1 Hz, oxygen partial pressure of 10^{-4} Torr, temperature of 680°C and energy density of 1.15 $\frac{J}{cm^2}$. After deposition, samples were cooled to room temperature at a rate of 3 $\frac{^\circ C}{min}$ at the deposition environment. The same growth procedure was followed for nonferroelectric LAO/ETO/STO interfaces studied here, varying only the thickness of the ETO layer. Back-gate electrodes were attached to the bottom of the CSTO with Ag paint. When gate voltage was applied, the leakage current was immeasurably small (<1 pA). The gate voltage is defined as positive when electrons accumulate at the interface. Measurements were performed in a PPMS system with a base temperature of 2 K and magnetic fields up to 14 T. Measurements below 2 K were conducted in a Triton dilution refrigerator with a base temperature of 20 mK.

B. Scanning SQUID Measurements

We use a scanning SQUID microscope with a micron size sensitive area (the pick-up loop). The pick-up loop is rastered above the surface of the sample, recording the Z component of the magnetic field as a function of position [30–33], in units of flux (Φ_0). Local magnetometry, susceptometry, and current response measurements were performed simultaneously. Magnetometry mode maps the static magnetic landscape, captured by the SQUID's pick-up loop. Susceptometry measurements are performed by applying local magnetic field with a field coil loop that surrounds the pick-up loop. In the data shown here ac current (0.1–3 mA RMS, 1–3 kHz) was applied to the field coil generates a local magnetic field of 0.1–3 G RMS. The pick-up loop detects magnetic signals generated by the applied field. This signal is separated from dc data by using a lock-in. To compensate for background magnetic fields an identical pick-up loop, surrounded by an identical field coil, is located 1.2 mm away and wired in a gradiometric design. Magnetic flux measured by the SQUID pick-up loop is converted to unitless susceptibility following Ref. [34] (see the Appendix in the Supplemental Material [22] for calculating the conversion coefficient for our SQUID). For mapping electric current flow, we capture the magnetic fields generated by the current by the pick-up loop. These signals are separated from others by using a lock-in. A thread of current flow appears in a SQUID image as a negative magnetic signal next to a positive signal. We perform all scans at a fixed sensor-sample distance of $\sim 1\ \mu m$.

V. SUMMARY

In this work, we explored magnetism, ferroelectricity and their interactions with the 2D electron system formed at the the $LaAlO_3/EuTiO_3/Sr_{0.99}Ca_{0.01}TiO_3$ interface. The conducting electrons in the 2DES experience magnetic scattering originating from the $EuTiO_3$ layer. This is evident from a diverging $ln(\frac{1}{T})$ term in the interface resistance appearing at low temperatures along with a Curie-Weiss-type behavior of the ETO susceptibility. By analyzing magnetoresistance measurements, we were able to separate out the contribution of the spin scattering to the magnetoresistance. This scattering component becomes dominant as temperature is lowered and is tunable by gate biasing, becoming stronger when electrons are depleted from the 2DES. Ferroelectricity also interacts with the 2DES as demonstrated by the hysteresis observed in sheet resistance when switching ferroelectric polarization in the bulk. Furthermore, magnetic scatterings were shown to be tuned by switchable ferroelectric memory.

While the 2DES interacts with both ferroelectricity and magnetism, we find that the presence of conduction electrons has no effect on the magnetic susceptibility of the $EuTiO_3$ layer. Furthermore, no signs of ferromagnetism is observed in any of our $EuTiO_3$-based samples with or without ferroelectricity. Control of ferromagnetism in this sort of ferroelectric/2DES/magnetic heterostructure is desired in order to realize a new type of multiferroic where ferroelectricity could control not only magnetic scatterings, but also magnetic memory. By selecting other magnetic materials it should be possible to achieve this desired functionality.

ACKNOWLEDGMENTS

Work in TAU (G.T, S.S and Y.D.) was supported by the Pazy Research Foundation Grant No. 326-1/22, Israeli Science Foundation Grant No. ISF-3079/20 and ISF-382/17, the TAU Quantum Research Center and the oren family chair for experimental physics. Work in BIU (S.W.S and B.K.) was supported by the European Research Council Grant No. ERC-2019-COG-866236, the Israeli Science Foundation Grant No. ISF-1281/17, and the Pazy Research Foundation Grant No. 107/18.

G.T. and S.W.S. contributed equally to this work. G.T. and Y.D. conceived the experiment, G.T and S.S fabricated samples, conducted magnetotransport and capacitance measurements. S.W.S and B.K. Performed the scanning-SQUID measurements. All authors analyzed the data and wrote the manuscript. We thank A. Yasuhara for conducting the STEM measurements. We thank A. Sirohi and N. Rotem for their help with the scanning SQUID measurements. We thank M. Salluzo and M. Bibes for useful discussions.

[1] N. A. Hill, J. Phys. Chem. B **104**, 6694 (2000).
[2] B. Matthias, J. Appl. Phys. **38**, 928 (1967).
[3] J. A. Mundy, C. M. Brooks, M. E. Holtz, J. A. Moyer, H. Das, A. F. Rébola, J. T. Heron, J. D. Clarkson, S. M. Disseler, Z. Liu *et al.*, Nature (London) **537**, 523 (2016).
[4] G. Tuvia, Y. Frenkel, P. K. Rout, I. Silber, B. Kalisky, and Y. Dagan, Adv. Mater. **32**, 2000216 (2020).
[5] T. McGuire, M. Shafer, R. Joenk, H. Alperin, and S. Pickart, J. Appl. Phys. **37**, 981 (1966).
[6] C.-L. Chien, S. DeBenedetti, and F. D. S. Barros, Phys. Rev. B **10**, 3913 (1974).

[7] V. Scagnoli, M. Allieta, H. Walker, M. Scavini, T. Katsufuji, L. Sagarna, O. Zaharko, and C. Mazzoli, Phys. Rev. B **86**, 094432 (2012).
[8] J. H. Lee, L. Fang, E. Vlahos, X. Ke, Y. W. Jung, L. F. Kourkoutis, J.-W. Kim, P. J. Ryan, T. Heeg, M. Roeckerath *et al.*, Nature (London) **466**, 954 (2010).
[9] K. S. Takahashi, M. Onoda, M. Kawasaki, N. Nagaosa, and Y. Tokura, Phys. Rev. Lett. **103**, 057204 (2009).
[10] K. Shimamoto, K. Hatabayashi, Y. Hirose, S. Nakao, T. Fukumura, and T. Hasegawa, Appl. Phys. Lett. **102**, 042902 (2013).
[11] Y. Kususe, H. Murakami, K. Fujita, I. Kakeya, M. Suzuki, S. Murai, and K. Tanaka, Jpn. J. Appl. Phys. **53**, 05FJ07 (2014).
[12] T. Katsufuji and Y. Tokura, Phys. Rev. B **60**, R15021 (1999).
[13] T. Yamamoto, R. Yoshii, G. Bouilly, Y. Kobayashi, K. Fujita, Y. Kususe, Y. Matsushita, K. Tanaka, and H. Kageyama, Inorg. Chem. **54**, 1501 (2015).
[14] K. Ahadi, L. Galletti, and S. Stemmer, Appl. Phys. Lett. **111**, 172403 (2017).
[15] K. Kugimiya, K. Fujita, K. Tanaka, and K. Hirao, J. Magn. Magn. Mater. **310**, 2268 (2007).
[16] P. Ryan, J. Kim, T. Birol, P. Thompson, J. Lee, X. Ke, P. Normile, E. Karapetrova, P. Schiffer, S. Brown *et al.*, Nat. Commun. **4**, 1334 (2013).
[17] K. S. Takahashi, H. Ishizuka, T. Murata, Q. Y. Wang, Y. Tokura, N. Nagaosa, and M. Kawasaki, Sci. Adv. **4**, eaar7880 (2018).
[18] D. Stornaiuolo, C. Cantoni, G. De Luca, R. Di Capua, E. D. Gennaro, G. Ghiringhelli, B. Jouault, D. Marrè, D. Massarotti, F. M. Granozio *et al.*, Nat. Mater. **15**, 278 (2016).
[19] A. Ohtomo and H. Hwang, Nature (London) **427**, 423 (2004).
[20] L. Yu and A. Zunger, Nat. Commun. **5**, 5118 (2014).
[21] S. Lemal, N. C. Bristowe, and P. Ghosez, Phys. Rev. B **102**, 115309 (2020).
[22] See Supplemental Material at http://link.aps.org/supplemental/10.1103/PhysRevMaterials.6.074408 for supporting information, including measurements on the nonferroelectric LAO/ETO/STO heterostructure.
[23] J. G. Bednorz and K. A. Müller, Phys. Rev. Lett. **52**, 2289 (1984).
[24] J. Bréhin, F. Trier, L. M. Vicente-Arche, P. Hemme, P. Noël, M. Cosset-Chéneau, J.-P. Attané, L. Vila, A. Sander, Y. Gallais, A. Sacuto, B. Dkhil, V. Garcia, S. Fusil, A. Barthelemy, M. Cazayous, and M. Bibes, Phys. Rev. Materials **4**, 041002(R) (2020).
[25] A. Millis, Nature (London) **392**, 147 (1998).
[26] E. Nagaev, Phys. Usp. **39**, 781 (1996).
[27] S. Finkelman, M. Sachs, G. Droulers, N. P. Butch, J. Paglione, P. Bach, R. L. Greene, and Y. Dagan, Phys. Rev. B **82**, 094508 (2010).
[28] P. Delugas, A. Filippetti, V. Fiorentini, D. I. Bilc, D. Fontaine, and P. Ghosez, Phys. Rev. Lett. **106**, 166807 (2011).
[29] N. Lebedev, M. Stehno, A. Rana, P. Reith, N. Gauquelin, J. Verbeeck, H. Hilgenkamp, A. Brinkman, and J. Aarts, Sci. Rep. **11**, 10726 (2021).
[30] M. E. Huber, N. C. Koshnick, H. Bluhm, L. J. Archuleta, T. Azua, P. G. Björnsson, B. W. Gardner, S. T. Halloran, E. A. Lucero, and K. A. Moler, Rev. Sci. Instrum. **79**, 053704 (2008).
[31] J. R. Kirtley, B. Kalisky, J. A. Bert, C. Bell, M. Kim, Y. Hikita, H. Y. Hwang, J. H. Ngai, Y. Segal, F. J. Walker, C. H. Ahn, and K. A. Moler, Phys. Rev. B **85**, 224518 (2012).
[32] B. W. Gardner, J. C. Wynn, P. G. Björnsson, E. W. Straver, K. A. Moler, J. R. Kirtley, and M. B. Ketchen, Rev. Sci. Instrum. **72**, 2361 (2001).
[33] E. Persky, I. Sochnikov, and B. Kalisky, Annu. Rev. Condens. Matter Phys. **13**, 385 (2022).
[34] H. Bluhm, J. A. Bert, N. C. Koshnick, M. E. Huber, and K. A. Moler, Phys. Rev. Lett. **103**, 026805 (2009).